ACS APPLIED MATERIALS & INTERFACES

Research Article

www.acsami.org

Stimuli-Responsive Polypropylene for the Sustained Delivery of TPGS and Interaction with Erythrocytes

Chunming Li,[†,‡] Jing Jin,*[,†] Jingchuan Liu,[†] Xiaodong Xu,[§] and Jinghua Yin*[,†]

[†]State Key Laboratory of Polymer Physics and Chemistry, Changchun Institute of Applied Chemistry, Chinese Academy of Sciences, Changchun 130022, P. R. China

[‡]Graduate University of Chinese Academy of Sciences, Beijing 100049, P. R. China

[§]Polymer Materials Research Center, College of Materials Science and Chemical Engineering, Harbin Engineering University, Harbin 150001, P. R. China

Supporting Information

ABSTRACT: Hemocompatibility and oxidative stress are significant for blood-contacting devices. In this study, *N*-isopropylacrylamide (NIPAAm) and *N*-(3-aminopropyl)methacrylamide hydrochloride (APMA) were cografted on polypropylene (PP) membrane using ultraviolet grafting to load antioxidative D-α-tocopheryl polyethylene glycol 1000 succinate (TPGS) and control the release of TPGS. The immobilization of NIPAAm and APMA onto PP membrane was confirmed by attenuated total reflectance Fourier-transform infrared spectroscopy and X-ray photoelectron spectroscopy. Combined with data from platelet adhesion, red blood cell (RBC) attachment, and hemolysis rate, the hemocompatibility of PP was significantly improved. An in-depth characterization using hemolysis rate test, scanning electron microscopy, atomic force microscopy, and confocal laser scanning microscopy was conducted to confirm that the mechanism of the release of TPGS interacted with RBCs was different at different stages. The release of TPGS from the loading PP membranes affected hemolysis at different stages. At the early stage of release, TPGS maintained the tiny (nanometer-sized) tubers on the membrane surface and enhanced the membrane permeabilization by generating nanosized pores on the cell membranes. Afterward, the incorporated TPGS slowed the lipid peroxidation of erythrocytes and filled in the lipid bilayer of erythrocyte to prevent hemolysis. Thus, the approach implemented to graft NIPAAm and APMA and load TPGS was suitable to develop medical device with excellent hemocompatibility and antioxidative property.

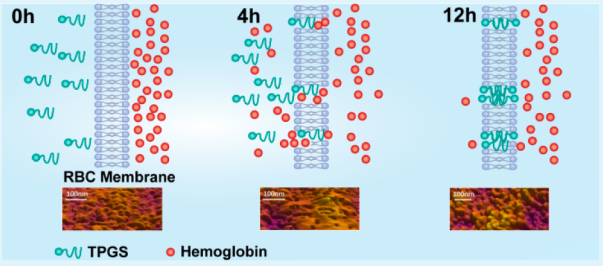

KEYWORDS: *polypropylene nonwoven fabric membrane, responsive polymer brush, controlled release, D-α-tocopheryl polyethylene glycol 1000 succinate, antioxidative*

1. INTRODUCTION

Hemocompatibility is one of the challenging problems for blood-contacting devices, such as artificial blood vessels, heart valves, hemodialysis membranes, and blood bags.[1] Polypropylene (PP) is one of the most promising blood-contacting devices because of its nontoxic and excellent mechanical properties. However, PP has poor blood compatibility. Numerous studies have focused on enhancing the hemocompatibility of PP surface, including antifouling properties, platelet activation, and contact activation.[2,3] Several strategies have been used to modify PP surfaces, such as γ-ray irradiation,[3] plasma discharge,[4] and UV-induced surface graft polymerization, which is particularly attractive because of its low cost, easy operation, simple equipment, and mild reaction conditions. In addition, UV graft polymerization improves the surface performance of the substrate without affecting its bulk properties. Some grafting monomers, such as oligoethylene glycol (OEG)- or polyethylene glycol (PEG)-based monomers,[5] amphiphiles,[6] biomolecules,[7] and stimuli-responsive monomers[8] have been used for improving the hemocompatibility of biomaterials. Poly(*N*-isopropylacrylamide) (PNIPAAm) is one of the most popular stimuli-responsive polymers that exhibits a lower critical solution temperature (LCST) of 32 °C in an aqueous solution.[9] Above 32 °C, the segments of PNIPAAm aggregate and exhibit hydrophobic property, whereas NIPAAm chains fully extend and hydrate, becoming water-soluble below 32 °C.[10] Therefore, the unusual behavior of NIPAAm can be exploited toward the controlled release of bioactive compounds such as drug and protein at specific temperatures for good hemocompatibility.[11]

Another important issue of blood-contacting devices, such as blood bags and hemodialysis membranes, is oxidative stress produced by reactive oxygen species (ROS) during blood preserving and hemodialysis.[12−14] Excess ROS causes damage to cell components.[15] Erythrocytes are frequently used to investigate the potential activity of antioxidants because they

Received: May 28, 2014
Accepted: July 22, 2014
Published: July 22, 2014

have high levels of polyunsaturated fatty acids (PUFA) in membranes. Erythrocytes exposed to excess ROS undergo cell lysis because of oxidative damage.[16] Therefore, ROS-inducing hemolysis is inhibited by several scavengers of oxygen-derived radicals, such as epicatechin,[17,18] *N*-allylsecoboldine,[19] tea polyphenols,[20] c-phycocyanin,[16] and vitamin E.[21] Previous studies have reported that vitamin E can improve the antioxidative activity of hemodialysis membrane.[22,23] Vitamin E protects cell membranes, especially in the lungs and red blood cells (RBCs), and resists damage caused by various pollutants, peroxides, and free radicals formed in metabolic processes. However, the antioxidative mechanism of vitamin E is rather controversial. Wagner et al. concluded that vitamin E inhibited lipid peroxidation in cells by slowing the rate of lipid peroxidation.[21] By contrast, Fang Wang et al. indicated that vitamin E had physicochemical membrane stabilizing effect in suppressing hemolysis induced by hemin.[24]

D-α-Tocopheryl polyethylene glycol 1000 succinate (TPGS) is formed by esterification of vitamin E succinate with polyethylene glycol (PEG) 1000, which is widely used as water-soluble vitamin E formulation. The U.S. Food and Drug Administration (FDA) has approved TPGS as a safe pharmaceutical adjuvant used in drug formulation.[25] Recently, polysulfone (Psf) membrane containing TPGS in single step has been fabricated.[26,27] Antioxidative Psf-TPGS exhibits enhanced biocompatibility, and the membranes show high flux and urea clearance. However, few studies have concentrated on the antioxidative property of PP used in blood-contact materials. Thus, the antioxidative property of long-term blood-contacting PP is important for the hemolysis of erythrocytes.

In this study, we fabricated dual-functional PP membranes by grafting stimuli-responsive monomers and loading controlled-release TPGS, which endowed PP with hemocompatibility and antioxidative performance. The mechanism of the effect of releasing TPGS on erythrocytes was investigated. The proposed method may be an easy and convenient way to evaluate the effect of TPGS molecules in a continuous releasing manner on cells.

2. EXPERIMENTAL SECTION

2.1. Materials. Polypropylene nonwoven fabric (PP NWF) membrane was obtained from Beijing JDKR Co., Ltd. (Beijing, China) with an average pore diameter of 0.22 μm. *N*-Isopropylacrylamide (NIPAAm), anhydrous dioxane, and acid blue 9 were obtained from J&K Chemical Ltd. Benzophenone (BP), *N*-(3-aminopropyl)-methacrylamide hydrochloride (APMA), D-α-tocopherol polyethylene glycol 1000 succinate (TPGS), 4-(dimethylamino)pyridine (DMAP), succinic anhydride (SA), and triethylamine (TEA) were purchased from Sigma-Aldrich chemical Co. 4,4-difluoro-5,7-dimethyl-4-bora-3a,4a-diaza-*S*-indacene-3-hexadecanoic acid (BODIPY FL C_{16}, C_{16}–BODIPY) was purchased from Molecular Probes (Eugene, OR, USA). Phosphate-buffered saline (PBS, 0.01 M phosphate buffer, pH 7.4) was prepared freshly. The other solvents and reagents were AR grade and used without further purification.

2.2. Preparation, Characterization, and Hemocompatibility of Modified PP Membranes. *2.2.1. Preparation of NIPAAm and APMA Modified Responsive Polymer Brush.* PP NWF membranes of 1 cm × 2 cm in size were washed with acetone for 12 h and cleaned with acetone for 30 min in an ultrasonic water bath. The films were dried under vacuum for 24 h at room temperature and weighed before use. The dry membranes were immersed in the ethanol solution of BP (1 wt %) for 30 min and dried at room temperature. Then the membrane was put on a quartz plate and coated with 50 μL of NIPAAm and APMA aqueous solution. Another quartz plate was covered on the membrane. The sandwiched system was exposed to UV light (high-pressure mercury lamp, 400 W, main wavelength = 380 nm) for a desired period. All the grafting membranes were washed with ethanol and water to remove residual monomer. The grafting degree (GD) of the membrane was calculated based on formula 1:

$$\mathrm{GD}(\mu\mathrm{g/cm^2}) = \frac{W_1 - W_0}{S} \quad (1)$$

where W_1 and W_0 are the weight (μg) of the modified and virgin membrane, respectively; S is the surface area (cm^2) of the membrane.

2.2.2. Surface Characterization. The surface chemical structure of the modified PP membranes was analyzed by Fourier transform infrared spectroscopy (FTIR, BRUKER Vertex 70) with an attenuated total reflection unit (ATR crystal, 45°) at a resolution of 4 cm^{-1} for 32 scans. The chemical composition of modified PP membranes were characterized by X-ray photoelectron spectroscopy (XPS, VG Scientific ESCA MK II Thermo Avantage V 3.20 analyzer) with Al/K ($h\nu$ = 1486.6 eV) anode mono-X-ray source. All the samples were completely vacuum-dried prior to use. The releasing angle of the photoelectron for each atom was fixed at 90°. Surface spectra were collected over a range of 0−1200 eV, and high-resolution spectra of C 1s, N 1s, O 1s, and Cl 1s regions were collected. The atomic concentrations of the elements were calculated by their corresponding peak areas.

2.2.3. Blood-Clotting Test. Fresh blood collected from a healthy rabbit was mixed immediately with a 3.8 wt % solution of sodium citrate at a dilution ratio of 9:1. (The experiments were carried out in accordance with the guidelines issued by the Ethical Committee of the Chinese Academy of Sciences.) The blood was centrifuged at 1000 rpm for 15 min to obtain the platelet-rich plasma (PRP). The membranes of pieces (1 cm × 1 cm) were incubated for 2 h in PBS and placed in a tissue culture plate. Then 50 μL of fresh PRP was dropped onto the center of the membrane and incubated at 37 °C for 60 min. The nonadhered platelets were rinsed by PBS three times. Subsequently, the platelet adhering to the membrane was fixed by 2.5 wt % glutaraldehyde at 4 °C for 10 h. Finally, the membranes were washed with PBS three times, dehydrated with a series of ethanol/water mixtures (30, 50, 70, 90, and 100 vol % ethanol; 30 min in each mixture), and then dried under vacuum. The surface of the membrane was gold-sputtered in vacuum and observed with field emission scanning electron microscopy (FESEM, XL 30 ESEM FEG, FEI Company).

2.2.4. Hemolysis Rate Test. Blood from rabbit was collected in tubes containing sodium citrate and used within 4 h. Erythrocytes were separated from plasma and lymphocytes by centrifugation (3000 g, 5 min) at 4 °C, washed three times with PBS and suspended in PBS. Pristine, modified, and loading PP membranes were immersed in 3 mL of erythrocytes PBS suspensions. The samples were incubated on thermostatic shaker for certain time at 37 °C, 130 r/min. Hemolysis was spectrophotometrically determined according to Ko et al.[28] This was calculated by comparing the absorption of a sample with that of a complete hemolysis sample at the same wavelength. After incubation at certain time, the suspensions were centrifuged (3000 g, 5 min). Absorption (A) of the supernatant was read at 540 nm. A complete hemolysis sample was treated with distilled water, and after centrifugation, absorption (B) was measured at the same wavelength. The percentage of hemolysis was then calculated as (A/B) × 100%. All the hemolysis experiments were done in triplicate.

For studying the morphological changes, RBCs of the control and the test samples at the end of the incubation period were fixed in 2.5% glutaraldehyde for 30 min and washed three times using PBS. Cells were dehydrated in increasing concentrations of ethanol (50%, 70%, 90%, 95%, and 100%) for 15 min each. The cell pellet was dropped onto glass coverslips, dried, and gold-sputtered in vacuum before viewing under field emission scanning electron microscopy (FESEM, XL 30 ESEM FEG, FEI Company).

2.3. Loading and Releasing. *2.3.1. Synthesis of Carboxyl-Terminated TPGS.* To introduce negative charge to TPGS, TPGS was activated by succinic anhydride through ring-opening reaction in the presence of DMAP according to the procedure given by Si-Shen

Feng.[29,30] TPGS (Mn = 1500, 0.75 g, 0.5 mmol), succinic anhydride (0.06 g, 0.6 mmol), DMAP (0.061 g, 0.5 mmol), and TEA (0.051 g, 0.5 mmol) were dissolved in 6 mL of anhydrous dioxane and stirred for 24 h at 40 °C. This reaction allows for ester bond formation between the carboxylic group of succinic anhydride and the hydroxyl-terminated TPGS. The solvent was completely evaporated in a rotary evaporator. The residue was dissolved in dichloromethane and filtered to remove unreacted succinic anhydride. After filtration, the solution was precipitated in anhydrous ether. The precipitated product carboxyl-terminated TPGS (TPGS-SA) was then freeze-dried. If not mentioned, TPGS loaded on the membranes stands for carboxyl-terminated TPGS in this paper.

2.3.2. Acid Blue 9 and TPGS Loading. Virgin and modified PP membranes were immersed in 5 mL of acid blue 9 (0.5 mg/mL) or TPGS (200 μg/mL) aqueous solution at 25 °C for 24 h. The membranes were washed quickly by 37 °C water three times after loading. The temperature is higher than LCST; the physical absorbed TPGS at outermost layer of PP at 37 °C was washed away, while the TPGS trapped in polymer brushes cannot be washed away. Finally, the loaded membranes were dried under argon before releasing.

2.3.3. Release of Acid Blue 9 and TPGS in PBS. The acid blue 9 loaded membranes were immersed into 5 mL of PBS at 37 °C in a 12-well plate. The releasing amount of acid blue 9 was monitored using Microplate reader at 690 nm (maximum absorption wavelength of acid blue 9). The concentration of released acid blue 9 was calculated from standard curve. In this work, we found that TPGS has intrinsic fluorescence in PBS solution. It was possible to quantitatively determine the amount of TPGS released in the solution. The fluorescence intensity was recorded on a fluorospectrophotometer (Hitachi F-7000 spectrophotometer). The amount of TPGS was also calculated from standard curve.

2.4. Atomic Force Microcopy Measurements. RBCs of the control and the test samples at the end of the incubation period were fixed in 0.25% glutaraldehyde for 30 min and washed three times using PBS. RBC suspensions were diluted with PBS to obtain final suspension at 0.1% (v/v) hematocrit. 50 μL of each suspension was placed on a clean glass slide, spread forward to create a thin film, and air-dried.

AFM studies were carried out with an Asylum MFP-3D (Asylum research, Santa Barbara, CA) AFM. Erythrocytes were imaged in tapping mode with a scan rate of 0.2 Hz by the use of silicon cantilevers with a resonant frequency of 70 kHz (Olympus, OMCL-AC240TS). Several independent samples were analyzed, and several areas were studied on each sample. The morphology of one cell was shown by the large images (8 × 8 μm), and higher-resolution images (1 × 1 μm) were collected of individual cells. The images were processed and analyzed using IGOR Pro 6.04 software.

2.5. Labeling of RBC for Confocal Fluorescence Microscopy. For labeling with C_{16}–BODIPY, 100 μL of packed RBCs were suspended in 3 mL of PBS and then mixed with 6 μL of C_{16}–BODIPY in ethanol (0.2% ethanol concentration, 0.8 μM final probe concentration). The cells were then incubated for 30 min at room temperature under continuous agitation.[31] The stained RBCs were washed three times with PBS to remove the excess and free C_{16}–BODIPY.

After the loading and unloading samples were incubated with stained RBCs, RBCs were fixed in 2.5% glutaraldehyde for 30 min and washed three times using PBS. The cell pellet was dropped onto glass coverslips and air-dried. All the samples were away from light. Confocal laser scanning microscopy (CARL ZEISS LSM 700, Germany) was used in our experiments. The excitation wavelength was 488 nm. The fluorescence signals were simultaneously using multitrack mode into two different channels using bandpass filters of 516 and 590 nm, respectively. Confocal laser scanning microscopy experiments were performed at room temperature.

3. RESULTS AND DISCUSSION

3.1. Preparation, Characterization, and Hemocompatibility of Modified PP Membranes. *3.1.1. Grafting of NIPAAm and APMA onto PP Membranes.* Grafting of NIPAAm and APMA onto PP membranes was carried out by surface photografting polymerization. Contreras-Garcia et al. have grafted NIPAAm and APMA onto PP membranes for loading antibiotics by preirradiation method.[32,33] In this study, an attractive method, namely, UV-induced surface graft polymerization, was used because of its low cost, easy operation, simple equipment, and mild reaction conditions. Importantly, the membranes were used to load antioxidative TPGS, and the interaction of TPGS and red blood cells was investigated. As shown in Scheme 1, the dual functional surface

Scheme 1. Schematic Representation of Polymerization of Monomers and Controlled Loading and Releasing of TPGS

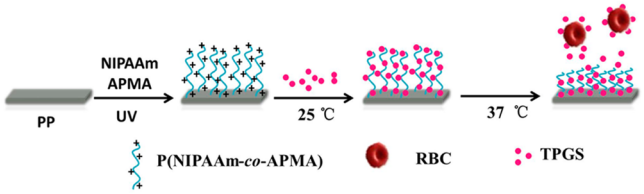

combined with NIPAAm and APMA was fabricated to load TPGS at room temperature, which was lower than the LCST of PNIPAAm. The release of loaded TPGS on PP membranes was controlled at 37 °C in blood to inhibit hemolysis of RBCs.

Figure 1A shows the ATR-FTIR spectra of the pristine and modified PP membranes after UV-grafting. A new peak appeared at 1647 and 1543 cm^{-1} in the PP-*g*-P(NIPAAm) spectra, which was assigned to the O═C−NH and N−H bands of PNIPAAm, respectively. The peak that appeared at 3301 cm^{-1} in the PP-*g*-P(NIPAAm) (Figure 1A(b)) spectrum was assigned to the characteristic amino (−NH−) bands of NIPAAm. After cografting with APMA, the peaks moved to lower wavenumbers at 1637 and 1539 cm^{-1}. The characteristic bands of APMA due to $-NH_3^+$ (2858−2610 cm^{-1}) as well as the peaks associated with −C−NH− groups (1043 and 1336 cm^{-1}) were not found in Figure 1A(c). The reason may be the small amount of APMA in brushes. We cannot clearly confirm the grafting of P(NIPAAm-*co*-APMA) brush only from ATR-FTIR. Combined with the data of XPS, we can confirm that APMA was successfully cografting on the surface of PP. After grafting of NIPAAm [Figure 1B(c)], the appearance of N 1s binding energy at 400 eV in the wide scan spectra confirmed the presence of PNIPAAm on the surface. The appearance of Cl 1s binding energy at 198 eV showed that APMA was successfully cografting on the surface of PP [Figure 1B(c)]. In Figure 1B, the N 1s core-level spectra were given. There was no nitrogen on virgin PP [Figure 1B(d)]. After grafting of NIPAAm, one N 1s peak at the binding energy of 399.5 eV was assigned to amide nitrogen (−N−C═O),[34] which confirmed the presence of PNIPAAm on the surface [Figure 1B(e)]. The C 1s core-level spectra of PP-*g*-P (NIPAAm-*co*-APMA) can be curve-fitted into two-peak component [Figure 1B(f)]. The two-peak components with binding energies at 399.5 and 401.2 eV were attributed to the amide nitrogen (−N−C═O) and the quaternary ammonium cations (N^+ species).[35] The existence of Cl 1s in wide-scan spectra and N^+ species in N 1s core-level spectra confirmed the APMA was successfully cografting on the surface of PP. In addition, the ratio between NIPAAm and APMA was estimated from the surface atom percentage of nitrogen and chlorine from XPS[36]

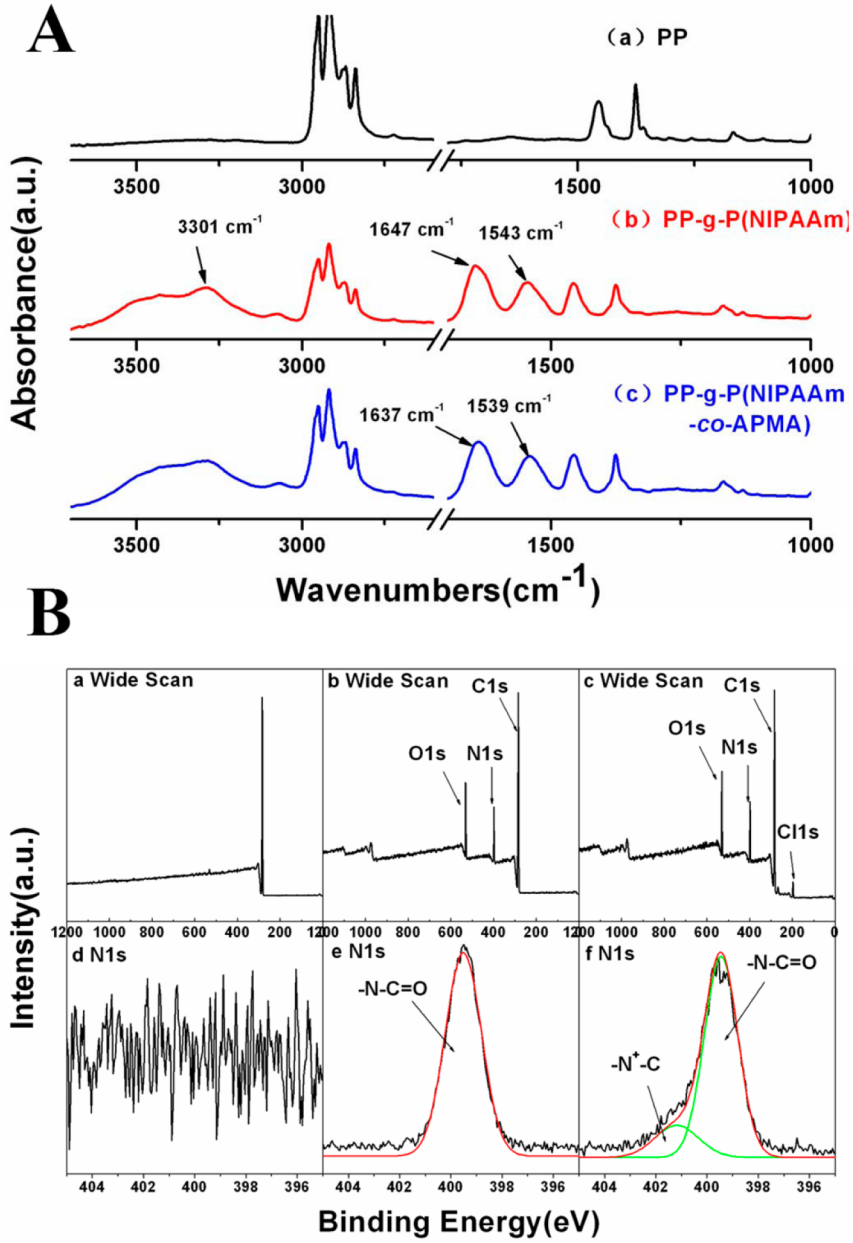

Figure 1. Characterization of PP and modified PP. (A) ATR-FTIR spectra of PP, PP-*g*-P (NIPAAm) and PP-*g*-P(NIPAAm-*co*-APMA). (B) Wide-scan and N 1s core-level spectra of (a, d) PP, (b, e) PP-*g*-P (NIPAAm), (c, f) PP-*g*-(NIPAAm-*co*-APMA).

because chlorine only comes from PAPMA, and the mole fraction of nitrogen is twice that of chlorine in pure APMA. The remaining N 1s only originated from PNIPAAm. The NIPAAm/APMA molar ratios can be calculated as follows:

$$\frac{M_{\mathrm{NIPAAm}}}{M_{\mathrm{APMA}}} = \frac{[\mathrm{N}] - 2[\mathrm{Cl}]}{[\mathrm{Cl}]} \qquad (2)$$

where $M_{\mathrm{NIPAAm}}/M_{\mathrm{APMA}}$ is the mole ratio of PNIPAAm and PAPMA in polymer brushes. [N] and [Cl] are the percentage of nitrogen and chlorine on modified surface determined by XPS, respectively. In Figure 1B(c), the percentage of N and Cl in PP-*g*-P (NIPAAm-*co*-APMA) was 12.76% and 2.38%, respectively; thus, NIPAAm/APMA was 3.36. The effect of grafting parameters on grafting degree is shown in Supporting Information, Figures S1 and S2.

3.1.2. Synthesis and Characterization of TPGS-SA. Hydroxyl-terminated TPGS was reacted with excess SA to introduce negative charge into TPGS. The structure of TPGS and TPGS-SA was detected by ^{1}H NMR in deuterated dimethyl sulfoxide (DMSO-d_6) (Figure 2A). The peak at 3.51 ppm was assigned to the $-CH_2$ protons of poly(ethylene oxide) part of TPGS. The lower peaks in the aliphatic region belonged to various moieties of vitamin E tails. ^{1}H NMR analysis of TPGS-SA demonstrated that the succinyl methylene (CH_2) gave signals at 2.3−2.4 ppm, as shown in the inset of Figure 2A. Besides, the peak at 4.55 ppm was not detected. The peak at 4.55 ppm was assigned to the −OH protons of TPGS. After reacting with succinic anhydride, ^{13}C NMR in DMSO-d_6 (Figure 3B) was also used to confirm the product identity. The ^{13}C NMR spectra of TPGS and TPGS-SA between 165 and 180 ppm are shown in Figure 2B. In this region, the peaks at 170.7 (a) and 171.9 (b) ppm were assigned to the two carboxyl carbon atoms in TPGS, while three peaks at 177.4 (f), 177.2 (d, e), and 176.0 (c) ppm appeared in the spectra of TPGS-SA.

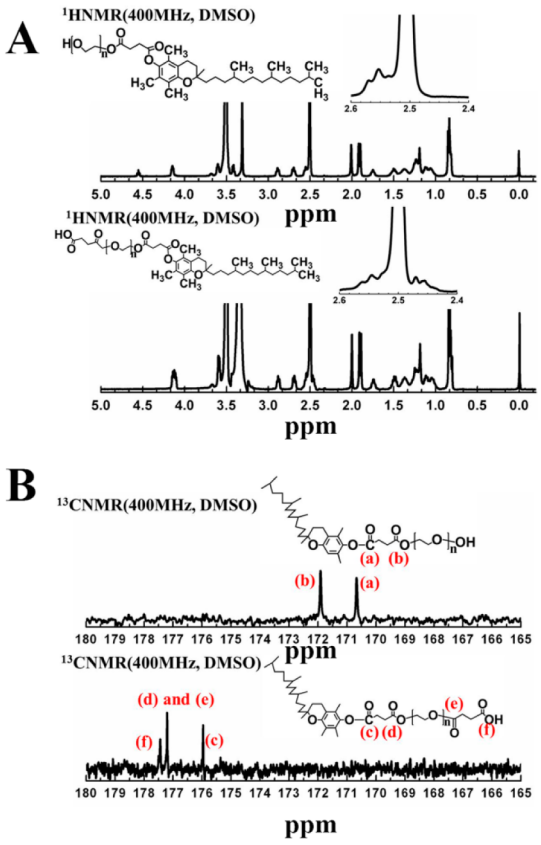

Figure 2. ^{1}HNMR spectra (A) and ^{13}C NMR spectra (B) of TPGS and TPGS-SA.

The two carboxyl carbon atoms connected to PEG segment (d, e) had the same chemical shift because they were in a similar chemical environment. The above results confirmed that the hydroxyl-terminated TPGS was transformed to carboxyl-terminated.

3.1.3. Hemocompatibility of Modified PP Membranes. When plasma protein is adsorbed on the biomaterial surface, platelets adhere, spread, and aggregate, which ultimately leads to thrombus formation.[37] Platelet adhesion and activation on material surface is an important parameter to evaluate the hemocompatibility of biomaterials.[38] Scanning electron microscopy (SEM) images of platelet adhesion of pristine PP, PP-*g*-P (NIPAAm), PP-*g*-P (NIPAAm-*co*-APMA), and PP-*g*-P (NIPAAm-*co*-APMA)-TPGS are shown in Figure 3A. A large amount of platelets adhered on the pristine PP surface [Figure 3A(a)], exhibiting highly activated with spread, aggregation, and pseudopodia states because of the high hydrophobic property of PP. In Figure 3A(b), the number of adhered platelets on the surface PP-*g*-P (NIPAAm) sharply decreased because of the hydration of PNIPAAm chains. However, a large number of platelets was found on the surface of PP-*g*-P (NIPAAm-*co*-APMA) [Figure 3A(c)], which is attributed to electrostatic attraction between positively charged APMA and negatively charged platelet. Studies showed that positive charge promoted erythrocyte adhesion[39] and platelet adhesion[40] but inhibited activation of the contact system.[41] Nearly no platelets were observed on the surface of TPGS-loading PP membranes [Figure 3A(d)]. On one hand, TPGS loading eliminated the positive charge on the membrane surface. The electrostatic interaction between membranes and platelets was reduced after loading. On the other hand, the release and diffusion of TPGS hindered platelet contact with membrane surface.

Furthermore, RBCs have relatively simple shapes, the transformation of which provides a sensitive response of cell-surface interactions.[42,43] The specific shape of cells on surfaces is determined by the interplay between the adhesion and the elastic properties of the membrane. Thus, the cell is attached to the surface when the adhesive energy is equal to or higher than the mechanical energy of the cell membrane. Figure 3B shows the erythrocyte adhesion of pristine PP, PP-*g*-P (NIPAAm-*co*-APMA), and TPGS loading PP. The specific adhesion of RBCs is disadvantageous to the application for blood-contacting materials. Different from platelets adhesion, the transmembrane proteins involved in the regulation and signal transduction in RBCs are nonadherent.[44] Interaction of RBCs with surfaces includes van der Waals interactions, electrostatic forces, bending undulations, and steric effects.[42,45] A number of erythrocytes adhere onto pristine PP (Figure 3B(a)) because of the hydrophobicity of PP. Several erythrocytes adhere on the PP-*g*-P (NIPAAm-*co*-APMA) surface [Figure 3B(b)]. Under physiological pH, the electrostatic interaction between negatively charged sialic acid residues and glycoproteins of the RBC glycocalyx and the positive charge of modified PP attracted erythrocytes onto the surface. The hemocompatibility of PP-*g*-P(NIPAAm) and PP-*g*-P(NIPAAm-*co*-APMA) at different grafting degrees was studied, and the results are shown in Supporting Information, Figure S3. Meanwhile, nearly no erythrocyte adhered on the TPGS-loading PP surface. The

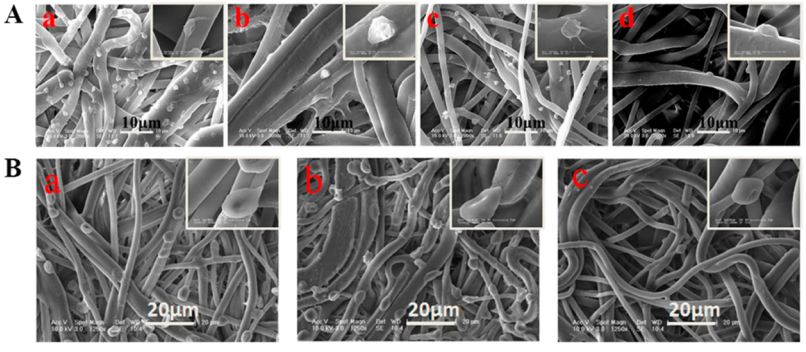

Figure 3. Hemocompatibilities of modified and loading PP membranes. (A) SEM images of platelet adhered on the surface of (a) PP, (b) PP-*g*-P(NIPAAm) with GD = 947.76 μg/cm^2, (c) PP-*g*-P(NIPAAm-*co*-APMA) with GD = 363.75 μg/cm^2, and (d) PP-*g*-P(NIPAAm-*co*-APMA)-TPGS (TPGS loading amount: 45.39 μg/cm^2). (B) SEM images of red blood cell adhered on the surface of (a) PP, (b) PP-*g*-P(NIPAAm-*co*-APMA) with GD = 363.75 μg/cm^2, and (c) PP-*g*-P(NIPAAm-*co*-APMA)-TPGS (TPGS loading amount: 45.39 μg/cm^2).

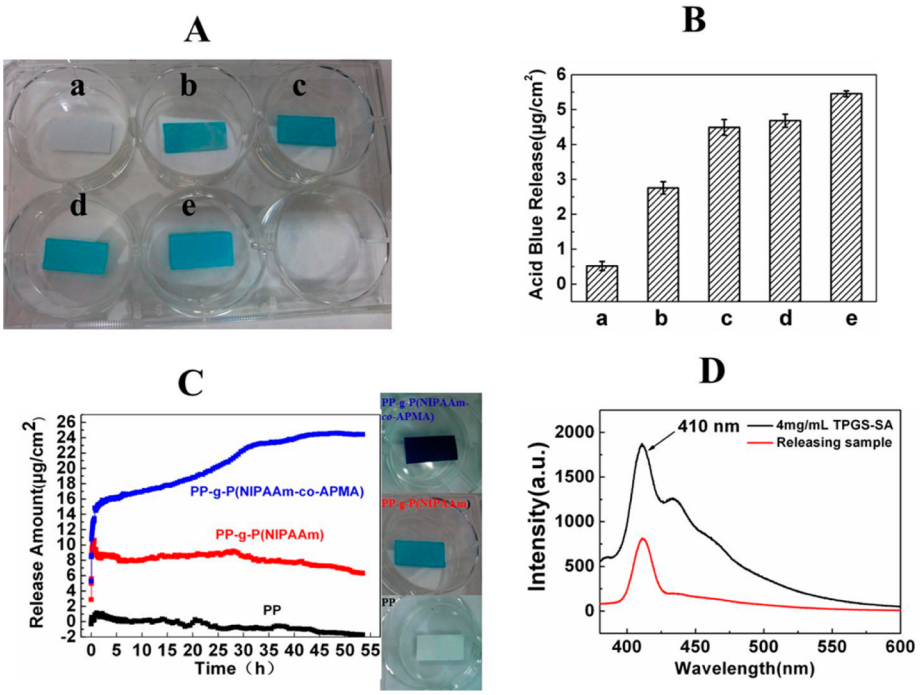

Figure 4. Loading and releasing of acid blue 9 and TPGS. (A, B) Acid blue 9 loading and releasing amount of PP-*g*-P(NIPAAm) with different grafting densities, (a) PP (b) 947.76 $\mu g/cm^2$ (c) 1549.04 $\mu g/cm^2$ (d) 1625.48 $\mu g/cm^2$ (e) 1926.12 $\mu g/cm^2$. (C) Acid blue 9 release profiles and loading pictures of the PP, PP-*g*-P (NIPAAm), and PP-*g*-P(NIPAAm-*co*-APMA). (D) Fluorescence emission spectra (excitation at 360 nm) of 4 mg/mL TPGS and PP-*g*-P (NIPAAm-*co*-APMA) releasing TPGS.

positive charge on PP membranes was eliminated after TPGS loading. TPGS-loading PP membranes reduced the contacting possibility of RBCs and PP membranes. Therefore, TPGS-loading PP membranes have excellent hemocompatibility for resisting platelet adhesion and RBC attachment.

3.2. Loading and Releasing. *3.2.1. Loading and Releasing of Acid Blue 9.* Acid blue 9 is an anionic dye used as a model to investigate the loading and release of modified PP membranes. The electrostatic interaction between the modified PP and acid blue 9, and the regulation of the releasing process, can be easily monitored. Figure 4A shows the loading and releasing amount of PP-*g*-P (NIPAAm) with different grafting densities. On the basis of the color after loading acid blue 9, the loading amount clearly increased with increased grafting density. The P (NIPAAm) brushes have the ability to absorb solvents.[46,47] Increasing the grafting density can enhance the ability to absorb much more solvent and acid blue 9. Figure 4B shows the quantitative amount of acid blue 9 releases. At the largest grafting density of PP-*g*-P (NIPAAm), the maximum loading amount can reach to 5.46 $\mu g/cm^2$.

3.2.2. Releasing Kinetics of Acid Blue 9. One of the most interesting features of PNIPAAm brushes as drug carriers is the temperature responsiveness of external changes. Thus, examining the release data from modified PP is significant. Drug release is regulated by swelling (at a temperature lower than the LCST) or shrinkage (at a higher temperature) of the polymer brushes. When the temperature rises above LCST, the polymer chain shrinks and aggregates because of the disruption of hydrogen bonding between the polymer chains and water molecules. The thickness of polymer brushes decreased, and the loading molecules released. Acid blue 9 release progress is shown in Figure 4C. Nearly no acid blue 9 was released from the pristine PP membranes. Acid blue 9 loaded on PP-*g*-P (NIPAAm) showed a releasing progress because of PNIPAAm shrinkage. Below LCST, the PNIPAAm chains form strong hydrogen bonds with water molecules and swell and expand in aqueous solution. When the temperature rises above LCST, the polymer shrinks and aggregates because of the disruption of hydrogen bonding between the polymer chains and water molecules. The releasing time of PP-*g*-P (NIPAAm) membrane was short for only half an hour. However, PP-*g*-P (NIPAAm-*co*-APMA) showed an important burst effect in half an hour and sustained released for 40 h. The controlled release can be attributed to the concomitant effects of (a) the shrinkage of the grafted copolymer at 37 °C, making diffusion slow; and (b) the strength of the ionic interactions between the acid blue 9 and the PAPMA. After 40 h, an equilibrium state between acid blue 9 immobilized in the grafted copolymer layer and dissolved in the medium is established. In addition, the amount of acid blue 9 released from PP-*g*-P(NIPAAm-*co*-APMA) was much higher than that released from PP-*g*-P(NIPAAm). Grafted APMA significantly promoted anionic molecule uptake. The above results indicated that APMA promoted molecule uptake and electrostatically interacted with anionic molecule to present a controlled release.

3.2.3. Loading and Releasing of TPGS. The key factor to monitor the release of TPGS is the detection method. Measuring the concentration of TPGS at a very low concentration using conventional method is difficult. Aranda F. J. et al. showed that the intrinsic fluorescence of α-tocopherol had been used as a tool to study the location and dynamics of the molecule in phospholipid vesicles.[48] In this study, TPGS-SA has intrinsic fluorescence in PBS solution. The amount of TPGS from the loading modified membranes can be quantitatively determined. The fluorescence intensity of 4 mg/mL and the release of TPGS from PP-*g*-P (NIPAAm-*co*-APMA) loading membrane are presented in Figure 4D. The excitation wavelength was at 360 nm and TPGS exhibited an

emission wavelength at 410 nm. The concentration of released TPGS was calculated from the standard curve of fluorescence intensity to concentration. The final release amount of TPGS-loading PP-*g*-P (NIPAAm-*co*-APMA) membrane was 45.39 μg/cm^2.

3.3. Effect of Releasing TPGS on Erythrocytes. *3.3.1. Effect of Releasing TPGS on Hemolysis.* Vitamin E has numerous functions, including anti-inflammatory, antithrombolytic, antioxidant, and other therapeutic effects.[49] Vitamin E also protects cell membranes, especially RBCs, against damage caused by free radicals formed during metabolic processes,[21] and it inhibits hemolysis. TPGS is a water-soluble form of vitamin E with an average molecular weight of about 1513, and it has been approved by the FDA as a drug solubilizer in oral, topical, parenteral, and rectal/vaginal therapies.[49,50] Figure 5

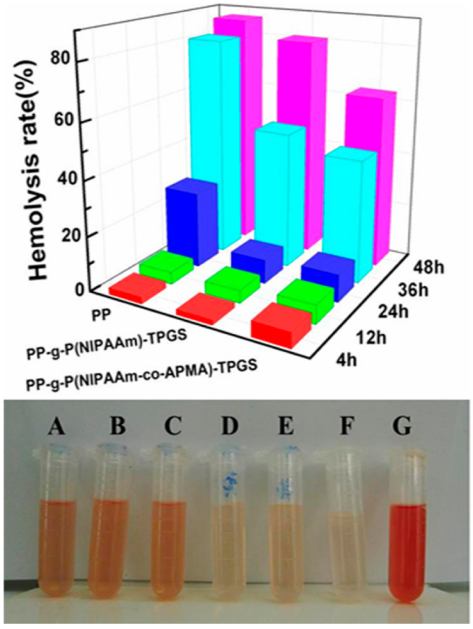

Figure 5. Hemolysis rates of PP and TPGS loading PP at different times in PBS (top) and the presence of hemoglobin in the supernatant was observed in (A) PP, (B) PP-*g*-P(NIPAAm), (C) PP-*g*-P(NIPAAm-*co*-APMA), (D) PP-*g*-P(NIPAAm)-TPGS, (E) PP-*g*-P(NIPAAm-*co*-APMA)-TPGS at 24h (bottom), (F) negative control, and (G) positive control.

(top) shows the hemolysis rates at different times of PP and TPGS-loading PP membranes. Before 12 h, the hemolysis rates of TPGS loading membranes (PP-*g*-P(NIPAAm)-TPGS and PP-*g*-P (NIPAAm-*co*-APMA)-TPGS) were a little higher than those of pristine PP. After 12 h, the hemolysis rates of TPGS-loading membranes were much lower than those of pristine PP. Furthermore, the hemolysis rate of PP-*g*-P (NIPAAm-*co*-APMA)-TPGS membrane was lower than that of PP-*g*-P (NIPAAm)-TPGS. The hemolysis rates increased with time for each sample because that oxygen radical was generated with time, which may cause lipid peroxidation and hemolysis. The image of hemolysis at 24 h is shown in Figure 5 (bottom). The loading membranes (D, E) had lower hemolysis than the corresponding unloading membranes (B, C). These results indicated that release of TPGS from the loading PP membranes effected hemolysis at different periods.

3.3.2. SEM Analysis of Erythrocytes. The morphology changes in erythrocytes were followed by SEM when TPGS-loading PP membranes contacted with blood. Figure 6 shows images of erythrocytes at different periods on different membranes. For the unloading PP membrane, all erythrocytes were transformed into echinocytes and lost their normal shape (Figure 6a,d,h), whereas erythrocytes maintained their normal discoid shapes and sizes for TPGS-loading membranes. In Figure 6, more echinocytes appeared over time for each sample because of peroxide stress. Rice-Evans[49] reported that echinocytes were produced by peroxide stress of erythrocyte. The shape of erythrocyte was sensitive to peroxidation by decreasing the fluidity of the lipid bilayer of the membranes.[51] Moreover, the percentage of normal-shaped erythrocytes increased after TPGS loading and decreased with time (Supporting Information, Figure S4), consistent with the results of the hemolysis. This result proved that TPGS prevented the original morphology changes of RBC and maintained the normal function of RBC in blood.

3.3.3. Membrane Topography Studies Using AFM. When pristine and TPGS-loading PP membranes contacted with blood, three-dimensional topographical images of RBCs using AFM are shown in Figure 7. Figure 7a,b shows the typically biconcave RBCs of control with smooth surfaces. A major change in cell morphology was observed for PP unloading sample (Figure 7c,d). However, the TPGS loading membranes maintained the normal discoid shape and size of RBCs (Figure 7e−h). The results were consistent with the SEM data.

Figure 8 shows a more detailed three-dimensional topography of RBC at higher magnification (1 μm × 1 μm). A well-organized and uniform nanosize tuber of an underlying cytoskeleton was observed on the normal RBC surface (Figure 8a), whereas obvious raised and depressed areas were found on the RBC surface of the unloading PP sample (Figure 8b); and a part of the nanometer tubers were disappeared. Raised and depressed areas are displayed on the RBC surface of TPGS-loading samples (Figure 8c,d). However, the tiny tubers of the nanometers are still maintained on the surface. For PP-*g*-P (NIPAAm-*co*-APMA)-TPGS, the RBC membrane appeared rough with numerous holes of a few nanometers (Figure 8e). D. R. Nogueira et al. concluded that surfactants changed the lipid−protein interactions in bilayer, which can be a biophysical mechanism directly related to membrane lysis.[52] TPGS is a synthetic amphiphile and safe surfactant. The holes observed on RBCs after TPGS release from AFM confirmed the effect of TPGS on the bilayer of RBCs. The surface roughness (RMS) of RBC was also measured from the high-resolution images, as shown in Figure 9. RMS values were consistent with the aforementioned images. The RMS values of the control RBC and the RBC of the PP sample were 2.19 and 4.03 nm, respectively, whereas the RBC RMS value of PP-*g*-P (NIPAAm)-TPGS was 4.54 nm. For PP-*g*-P (NIPAAm-*co*-APMA)-TPGS, the RMS value of RBC was 8.22 nm, higher than the size of hemoglobin (6.4 nm × 5.5 nm × 5.0 nm[53]). The AFM cross-sectional analysis of different samples is also shown in Supporting Information, Figure S5. Combined with the hemolysis rate test, the formation of holes and increase in RMS value may promote the hemoglobin transfer from erythrocyte in a short period. Therefore, at the early stage of release, TPGS maintained the tiny tubers of nanometers on the membrane surface and enhanced the membrane permeabilization by generating nanosize pores on the cell membranes.

3.3.4. TPGS Inhibits Lipid Peroxidation of Erythrocytes. Erythrocytes are abundant in membrane proteins and polyunsaturated fatty acids, and they have high cellular

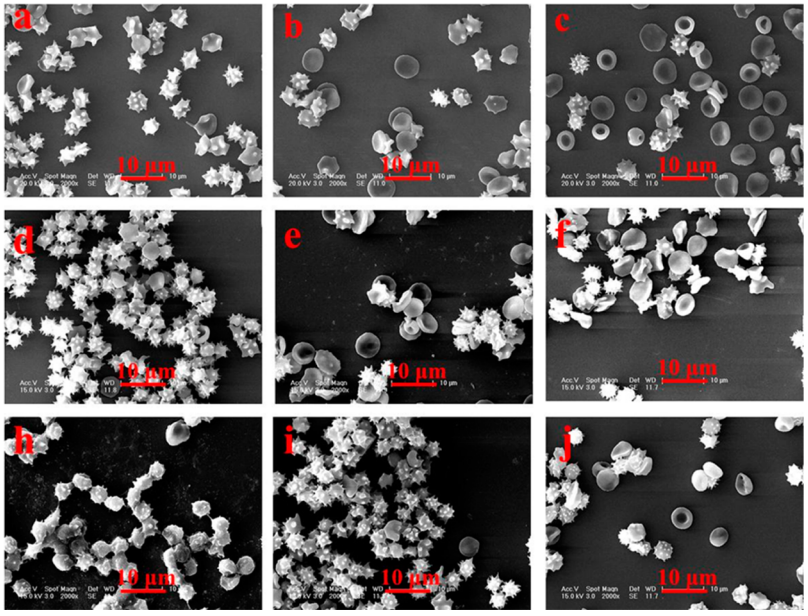

Figure 6. SEM images of RBC of (a,d,h) PP at 12 h, 24 h, 36 h, (b,e,i) PP-*g*-P(NIPAAm)-TPGS at 12 h, 24 h, 36 h, (c,f,j) PP-*g*-P(NIPAAm-*co*-APMA)-TPGS at 12 h, 24 h, 36 h.

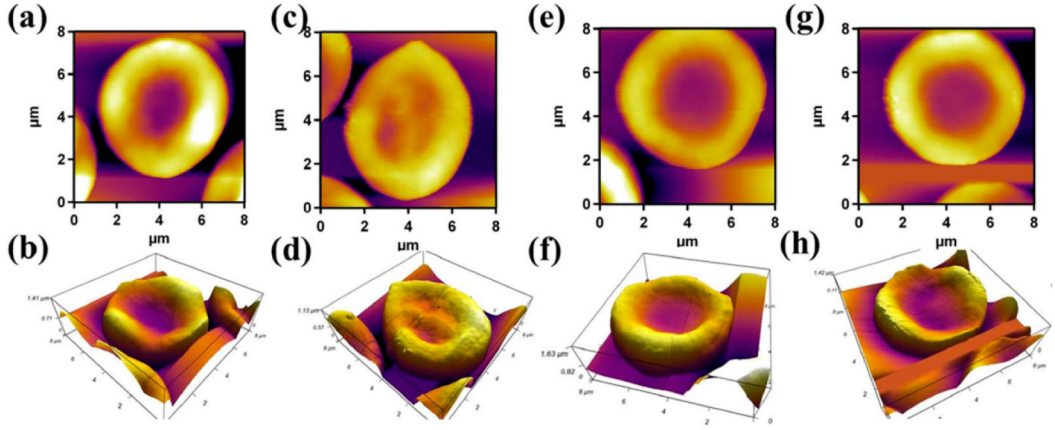

Figure 7. AFM images (8 μm × 8 μm) of RBCs of control (a, b), PP unloading samples (c, d), PP-*g*-P(NIPAAm)-TPGS (e, f), PP-*g*-P(NIPAAm-*co*-APMA)-TPGS (g, h) at 4h.

concentration of hemoglobin, iron, and oxygen.[18] Erythrocytes are highly susceptible to oxidative stress. Oxygen radical generating systems would cause hemolysis and lipid peroxidation. Studies[31,54,55] have shown that BODIPY-FL-based dyes can be adapted to a sensitive method to monitor lipid peroxidation. G. M. Makrigiorgos reported that the ratio of fluorescence intensities at 590 and 516 nm provided the most sensitive measure of lipid peroxidation, and the ratio decreased with lipid peroxidation.[30] Confocal laser scanning microscopy of erythrocytes stained with C_{16}–BODIPY (Figure 9) allowed visualization of the lipid of erythrocytes and comparison of the degree of lipid peroxidation. Images were generated with λ_{ex} = 488 nm, simultaneously recording in the green and red channels. The statistical analysis of the ratio of intensities at 590 and 516 nm at 24 h is shown in Figure 9 (right). TPGS loading samples have larger I_{590}/I_{516} than that of unloading PP, indicating that the RBCs contacting with TPGS loading PP undergo minimal lipid oxidation peroxidation at long time. Thus, at the second stage of release, TPGS released from the modified PP membranes slowed the lipid peroxidation of erythrocytes.

3.4. Mechanism of the Effect of Releasing TPGS on Erythrocytes. Oxidative stress is a vital indicator for induced cellular toxicity.[56,57] ROS, such as hydrogen peroxide, organo peroxide, superoxide anion, and hydroxyl radical are generated in biological systems and by exogenous sources. Excess ROS or loss of detoxification ability can lead to oxidative stress, which subsequently causes damage to cell components, including lipids, proteins, and cell membrane. Erythrocytes are used as a model to investigate the potential activity of antioxidants, the preferential physiological targets of ROS, because of a high level of PUFA in their membranes. Furthermore, erythrocytes carry high levels of intracellular oxygen and irons, which are important catalysts of oxidation reactions. Many antioxidants are used to suppress oxidative stress.[58] In addition, vitamin E is a chain-breaking antioxidant for preventing lipid peroxidation and stabilizing biological membranes by restricting the mobility of their components.[21] The mechanism of the protective effect of vitamin E on erythrocytes against hemolysis is shown in

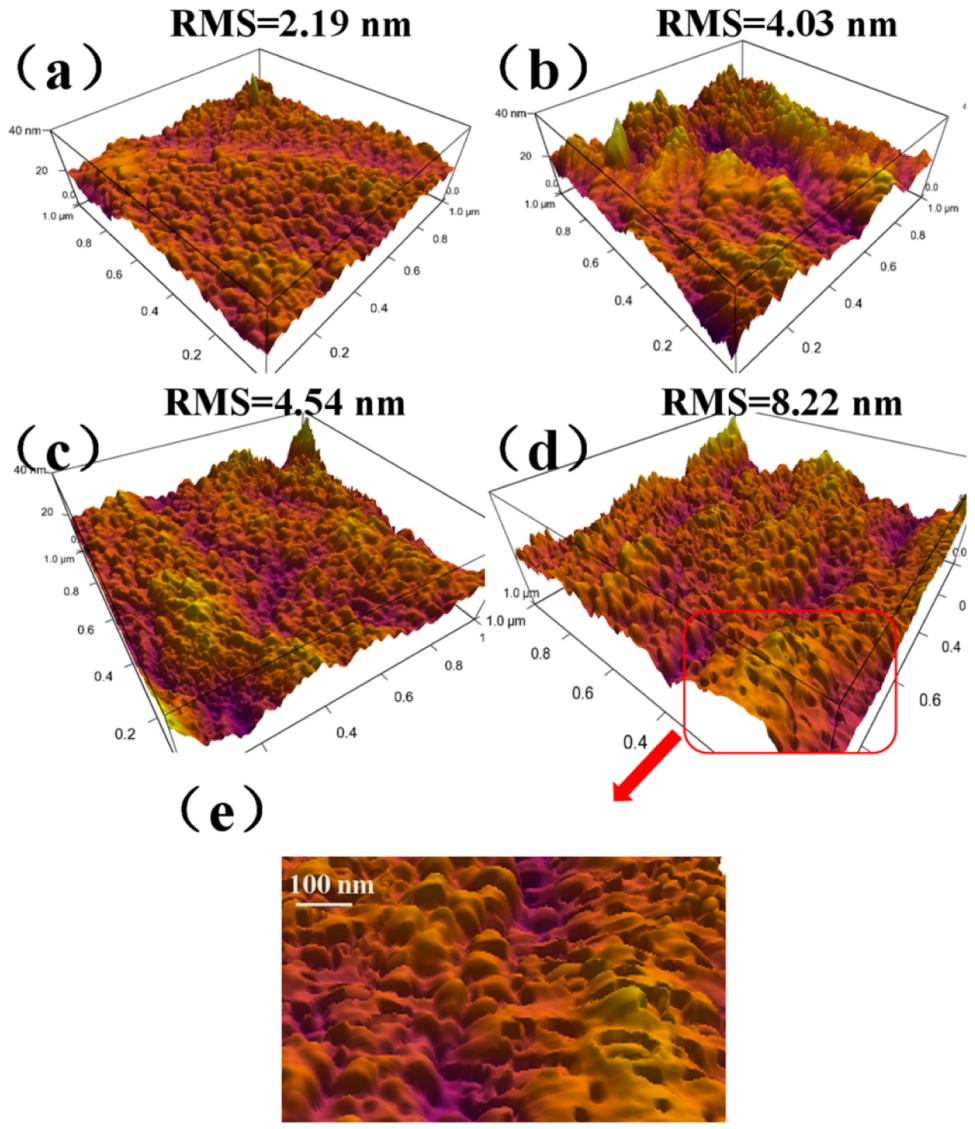

Figure 8. AFM images of the membrane surface of red blood cell (1 μm × 1 μm) for (a) control, (b) PP unloading sample, (c) PP-*g*-P(NIPAAm)-TPGS, (d) PP-*g*-P(NIPAAm-*co*-APMA)-TPGS, and (e) local enlarged image of PP-*g*-P(NIPAAm-*co*-APMA)-TPGS.

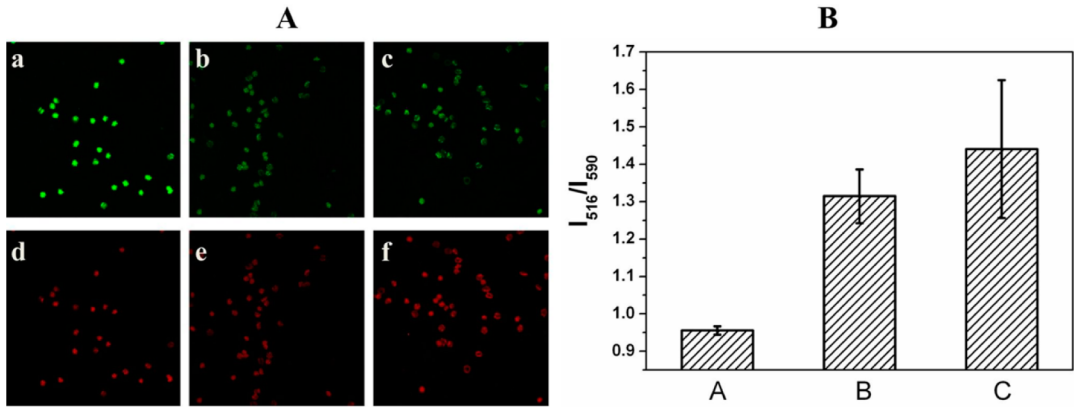

Figure 9. (A) LCSM images generated with λ_{ex} = 488 nm of RBC, stained with C_{16}–BODIPY of (a, d) PP, (b, e) PP-*g*-P (NIPAAm)-TPGS, (c, f) PP-*g*-P (NIPAAm-*co*-APMA)-TPGS with simultaneous recording in the green (λ_{em} = 516 nm) and red channels (λ_{em} = 590 nm). (B) Fluorescence intensity ratio of RBC, stained with C_{16}–BODIPY of λ_{em} = 590 nm and λ_{em} = 516 nm of (A) PP, (B) PP-*g*-P(NIPAAm)-TPGS, (C) PP-*g*-P(NIPAAm-*co*-APMA)-TPGS.

Scheme 3. At the early stage of release, the hemolysis of TPGS loading PP was a little higher than that of unloading samples. In Scheme 2 (middle), the released TPGS slightly induced RBC hemolysis. This effect can be explained by the amphipathy of

dx.doi.org/10.1021/am503332z | *ACS Appl. Mater. Interfaces* 2014, 6, 13956–13967

Scheme 2. Proposed Mechanism of the Interaction between Releasing TPGS and RBCs

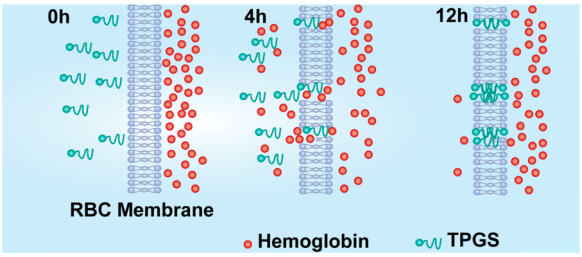

TPGS, which can be incorporated into membranes to enhance the permeabilization of erythrocyte. TPGS is one of the novel nonionic surfactants with an amphiphilic structure of lipophilic alkyl tail and hydrophilic polar head with a hydrophilic/lipophilic, which can be proved by the AFM data. The AFM data showed that the tiny tubers of nanometers on RBCs were maintained by the TPGS loading samples, whereas some tubers of nanometers on RBCs of PP unloading samples disappeared, illustrating that TPGS was incorporated into erythrocyte membranes. In addition, the nanosized pores in the cell membranes were observed, which helped elucidate the surfactant-induced membrane permeabilization. By combining the RBC hemolysis results and AFM data, we stated that TPGS was incorporated into erythrocyte membranes and enhanced the membrane permeabilization at the beginning of the release.

In Scheme 2 (left), the release of TPGS decreased the hemolysis and prevented the morphology changes of erythrocytes at the second stage of release. The mechanistic understanding of surfactant-induced membrane destabilization was investigated by D. R. Nogueira et.al.[52] The mechanism of biomembrane lysis is associated with lipid bilayer disorganization, through interaction with the lipids and proteins of the membrane. The incorporated TPGS slowed down the lipid peroxidation of erythrocytes and filled in the lipid bilayer of erythrocyte to prevent hemolysis. The SEM analysis of RBCs showed that TPGS prevented the morphology changes of erythrocytes. The morphological studies of RBCs at 12 h using AFM (Supporting Information, Figure S6) also showed that TPGS prevented the morphology changes of erythrocytes and maintained nanosize tubers of the membrane surface. The morphology protection by TPGS may be caused by the incorporation of TPGS into the area vacated by lipid.[24,59,60] Erythrocytes are susceptible to oxidative damage as a result of the high PUFA content of their membranes and the high cellular concentrations of oxygen and hemoglobin, a potentially powerful promoter of oxidative processes.[14,61] Even under normal conditions, erythrocytes are continuously exposed to ROS. Given that lipid peroxidation is one of the consequences of oxidative damage, RBC lipid peroxidation may be involved in normal cell aging and hemolysis. Along with time, autoxidation cannot be held by the cell itself. After 12 h, the hemolysis of TPGS-loading membranes was much lower than that of the unloading sample. This result can be explained by the antioxidative mechanism of the incorporated TPGS in cell membrane. The antioxidative mechanism was substantiated by the lipid peroxidation test. The fluorescence intensity variation of C_{16}–BODIPY confirmed that TPGS release from the modified PP membranes slowed the lipid peroxidation of erythrocytes. Therefore, the release of TPGS that interacted with RBC is a stepwise process. At the early stage of release, TPGS maintained the tiny (nanometer-sized) tubers on the membrane surface and enhanced membrane permeabilization by generating nanosize pores on the cell membranes. Afterward, the incorporated TPGS slowed the lipid peroxidation of erythrocytes and filled in the lipid bilayer of erythrocyte to prevent hemolysis.

4. CONCLUSION

In this study, PP was surface modified with NIPAAm and APMA by UV-induced graft polymerization. ATR-FTIR and XPS confirmed that the surface modification was successful. Carboxyl-terminated TPGS was synthesized and confirmed by ^{1}H NMR and ^{13}C NMR. PP-P (NIPAAm-*co*-APMA) was able to load TPGS and control its release under physiological conditions. The release of TPGS decreased hemolysis and prevented the morphology changes of erythrocytes obviously after 12 h but increased hemolysis a little at the beginning of the release. The mechanism of the interaction between releasing TPGS and erythrocytes was proposed. At the beginning of release, TPGS was incorporated into erythrocyte membranes and enhanced the membrane permeabilization. Afterward, the incorporated TPGS slowed the lipid peroxidation of erythrocytes. Therefore, the approach implemented to graft NIPAAm and APMA and load TPGS was suitable to develop medical device with excellent hemocompatibility and antioxidative property.

■ ASSOCIATED CONTENT

Ⓢ Supporting Information

The effects of grafting parameters on grafting degree; the effect of grafting degree on hemocompatibility; the percentage of discocyte in total erythrocytes; AFM cross-sectional analysis of different samples, and membrane topographies at 12 h. This material is available free of charge via the Internet at http://pubs.acs.org.

■ AUTHOR INFORMATION

Corresponding Authors

*E-mail: jjin@ciac.ac.cn. Fax: +86-431-85262126. Phone: +86-431-85262971. (J.J.)

*E-mail: yinjh@ciac.ac.cn. (J.H.Y.)

Notes

The authors declare no competing financial interest.

■ ACKNOWLEDGMENTS

The authors acknowledge the financial support of the National Natural Science Foundation of China (Project Nos. 51303178, 51103030, 51273199, and 21274150).

■ REFERENCES

(1) Zhang, Z.; Zhang, M.; Chen, S. F.; Horbetta, T. A.; Ratner, B. D.; Jiang, S. Y. Blood Compatibility of Surfaces with Superlow Protein Adsorption. *Biomaterials* **2008**, *29*, 4285–4291.

(2) Goli, K. K.; Rojas, O. J.; Genzer, J. Formation and Antifouling Properties of Amphiphilic Coatings on Polypropylene Fibers. *Biomacromolecules* **2012**, *13*, 3769–3779.

(3) Chen, S. H.; Chang, Y.; Lee, K. R.; Wei, T. C.; Higuchi, A.; Ho, F. M.; Tsou, C. C.; Ho, H. T.; Lai, J. Y. Hemocompatible Control of Sulfobetaine-Grafted Polypropylene Fibrous Membranes in Human Whole Blood via Plasma-Induced Surface Zwitterionization. *Langmuir* **2012**, *28*, 17733–42.

(4) Ferraz, C. C.; Varca, G. H.; Ruiz, J.-C.; Lopes, P. S.; Mathor, M. B.; Lugão, A. B.; Bucio, E. Radiation-Grafting of Thermo-and pH-

Responsive Poly (N-Vinylcaprolactam-Co-Acrylic Acid) onto Silicone Rubber and Polypropylene Films for Biomedical Purposes. *Radiat. Phys. Chem.* **2014**, *97*, 298−303.
(5) Hou, X.; Zhang, T.; Cao, A. A Heparin Modified Polypropylene Non-Woven Fabric Membrane Adsorbent for Selective Removal of Low Density Lipoprotein from Plasma. *Polym. Adv. Technol.* **2013**, *24*, 660−667.
(6) Fristrup, C. J.; Jankova, K.; Eskimergen, R.; Bukrinsky, J. T.; Hvilsted, S. Protein Repellent Hydrophilic Grafts Prepared by Surface-Initiated Atom Transfer Radical Polymerization from Polypropylene. *Polym. Chem.* **2012**, *3*, 198−203.
(7) Chang, Y.; Chang, W.-J.; Shih, Y.-J.; Wei, T.-C.; Hsiue, G.-H. Zwitterionic Sulfobetaine-Grafted Poly(vinylidene fluoride) Membrane with Highly Effective Blood Compatibility via Atmospheric Plasma-Induced Surface Copolymerization. *ACS Appl. Mater. Interfaces* **2011**, *3*, 1228−1237.
(8) Salas, C.; Genzer, J.; Lucia, L. A.; Hubbe, M. A.; Rojas, O. J. Water-Wettable Polypropylene Fibers by Facile Surface Treatment Based on Soy Proteins. *ACS Appl. Mater. Interfaces* **2013**, *5*, 6541−6548.
(9) Choi, B.-c.; Choi, S.; Leckband, D. E. Poly(*N*-isopropyl acrylamide) Brush Topography: Dependence on Grafting Conditions and Temperature. *Langmuir* **2013**, *29*, 5841−5850.
(10) Lin, X.; Tang, D.; Yu, Z.; Feng, Q. Stimuli-Responsive Electrospun Nanofibers from Poly(*N*-isopropylacrylamide)-*co*-Poly (Acrylic Acid) Copolymer and Polyurethane. *J. Mater. Chem. B* **2014**, *2*, 651−658.
(11) Gao, Y.; Zago, G. P.; Jia, Z.; Serpe, M. J. Controlled and Triggered Small Molecule Release from a Confined Polymer Film. *ACS Appl. Mater. Interfaces* **2013**, *5*, 9803−9808.
(12) Morena, M.; Delbosc, S.; Dupuy, A.-M.; Canaud, B.; Cristol, J.-P. Overproduction of Reactive Oxygen Species in End-Stage Renal Disease Patients: A Potential Component of Hemodialysis-Associated Inflammation. *Hemodial. Int.* **2005**, *9*, 37−46.
(13) Ward, R. A.; McLeish, K. R. Oxidant Stress in Hemodialysis Patients: What Are the Determining Factors? *Artif. Organs* **2003**, *27*, 230−236.
(14) Clemens, M. R.; Waller, H. D. Lipid Peroxidation in Erythrocytes. *Chem. Phys. Lipids* **1987**, *45*, 251−268.
(15) Aruoma, O. Oxidative Stress, and Antioxidants in Human Health and Disease. *J. Am. Oil Chem. Soc.* **1998**, *75*, 199−212.
(16) Pleonsil, P.; Soogarun, S.; Suwanwong, Y. Anti-Oxidant Activity of Holo- and Apo-C-Phycocyanin and Their Protective Effects on Human Erythrocytes. *Int. J. Biol. Macromol.* **2013**, *60*, 393−398.
(17) Martínez, V.; Ugartondo, V.; Vinardell, M. P.; Torres, J. L.; Mitjans, M. Grape Epicatechin Conjugates Prevent Erythrocyte Membrane Protein Oxidation. *J. Agric. Food Chem.* **2012**, *60*, 4090−4095.
(18) Ugartondo, V.; Mitjans, M.; Torres, J. L. s.; Vinardell, M. a. P. Biobased Epicatechin Conjugates Protect Erythrocytes and Non-tumoral Cell Lines from H_2O_2-Induced Oxidative Stress. *J. Agric. Food Chem.* **2009**, *57*, 4459−4465.
(19) Teng, C.-M.; Hsiao, G.; Ko, F.-N.; Lin, D.-T.; Lee, S.-S. *N*-Allylsecoboldine as a Novel Antioxidant against Peroxidative Damage. *Eur. J. Pharmacol.* **1996**, *303*, 129−139.
(20) Grinberg, L. N.; Newmark, H.; Kitrossky, N.; Rahamim, E.; Chevion, M.; Rachmilewitz, E. A. Protective Effects of Tea Polyphenols against Oxidative Damage to Red Blood Cells. *Biochem. Pharmacol.* **1997**, *54*, 973−978.
(21) Wagner, B. A.; Buettner, G. R.; Burns, C. P. Vitamin E Slows the Rate of Free Radical-Mediated Lipid Peroxidation in Cells. *Arch. Biochem. Biophys.* **1996**, *334*, 261−267.
(22) Sasaki, M. Development of Vitamin E-Modified Polysulfone Membrane Dialyzers. *J. Artif. Organs* **2006**, *9*, 50−60.
(23) Yamamoto, K.-i.; Matsuda, M.; Okuoka, M.; Yakushiji, T.; Fukuda, M.; Miyasaka, T.; Matsumoto, Y.; Sakai, K. Antioxidation Property of Vitamin E-Coated Polysulfone Dialysis Membrane and Recovery of Oxidized Vitamin E by Vitamin C Treatment. *J. Membr. Sci.* **2007**, *302*, 115−118.
(24) Wang, F.; Wang, T. H.; Lai, J. H.; Li, M.; Zou, C. G. Vitamin E Inhibits Hemolysis Induced by Hemin as a Membrane Stabilizer. *Biochem. Pharmacol.* **2006**, *71*, 799−805.
(25) Zhang, Z.; Tan, S.; Feng, S.-S. Vitamin E TPGS as a Molecular Biomaterial for Drug Delivery. *Biomaterials* **2012**, *33*, 4889−4906.
(26) Dahe, G. J.; Teotia, R. S.; Kadam, S. S.; Bellare, J. R. The Biocompatibility and Separation Performance of Antioxidative Polysulfone/Vitamin E TPGS Composite Hollow Fiber Membranes. *Biomaterials* **2011**, *32*, 352−365.
(27) Dahe, G. J.; Kadam, S. S.; Sabale, S. S.; Kadam, D. P.; Sarkate, L. B.; Bellare, J. R. In Vivo Evaluation of the Biocompatibility of Surface Modified Hemodialysis Polysulfone Hollow Fibers in Rat. *PLoS One* **2011**, *6*, e25236.
(28) Ko, F. N.; Hsiao, G.; Kuo, Y. H. Protection Of Oxidative Hemolysis By Demethyldiisoeugenol In Normal and β-Thalassemic Red Blood Cells. *Free Radical Biol. Med.* **1997**, *22*, 215−222.
(29) Zeng, X.; Tao, W.; Mei, L.; Huang, L.; Tan, C.; Feng, S.-S. Cholic Acid-Functionalized Nanoparticles of Star-Shaped PLGA-Vitamin E Tpgs Copolymer for Docetaxel Delivery to Cervical Cancer. *Biomaterials* **2013**, *34*, 6058−6067.
(30) Zhang, Z.; Feng, S. S. Nanoparticles of Poly(Lactide)/Vitamin E TPGS Copolymer for Cancer Chemotherapy: Synthesis, Formulation, Characterization and in Vitro Drug Release. *Biomaterials* **2006**, *27*, 262−70.
(31) Makrigiorgos, G. M. Detection of Lipid Peroxidation on Erythrocytes Using the Excimer-Forming Property of a Lipophilic Bodipy Fluorescent Dye. *J. Biochem. Biophys. Methods* **1997**, *35*, 23−35.
(32) Contreras-García, A.; Bucio, E.; Concheiro, A.; Alvarez-Lorenzo, C. Polypropylene Grafted with NIPAAm and APMA for Creating Hemocompatible Surfaces that Load/Elute Nalidixic Acid. *React. Funct. Polym.* **2010**, *70*, 836−842.
(33) Contreras-García, A.; Alvarez-Lorenzo, C.; Taboada, C.; Concheiro, A.; Bucio, E. Stimuli−Responsive Networks Grafted onto Polypropylene for the Sustained Delivery of NSAIDs. *Acta Biomater.* **2011**, *7*, 996−1008.
(34) Yang, B.-X.; Shi, J.-H.; Pramoda, K. P.; Goh, S. H. Enhancement of the Mechanical Properties of Polypropylene Using Polypropylene-grafted Multiwalled Carbon Nanotubes. *Compos. Sci. Technol.* **2008**, *68*, 2490−2497.
(35) Deng, S.; Zheng, Y. Q.; Xu, F. J.; Wang, B.; Huang, J.; Yu, G. Highly Efficient Sorption of Perfluorooctane Sulfonate and Perfluorooctanoate on a Quaternized Cotton Prepared by Atom Transfer Radical Polymerization. *Chem. Eng. J.* **2012**, *193*−*194*, 154−160.
(36) Cai, T.; Neoh, K. G.; Kang, E. T.; Teo, S. L. M. Surface-Functionalized and Surface-Functionalizable Poly(vinylidene fluoride) Graft Copolymer Membranes via Click Chemistry and Atom Transfer Radical Polymerization. *Langmuir* **2011**, *27*, 2936−2945.
(37) Sivaraman, B.; Latour, R. A. The Relationship between Platelet Adhesion on Surfaces and the Structure Versus the Amount of Adsorbed Fibrinogen. *Biomaterials* **2010**, *31*, 832−839.
(38) Spijker, H. T.; Bos, R.; Busscher, H. J.; van Kooten, T. G.; van Oeveren, W. Platelet Adhesion and Activation on a Shielded Plasma Gradient Prepared on Polyethylene. *Biomaterials* **2002**, *23*, 757−766.
(39) He, Q.; Gong, K.; Ao, Q.; Ma, T.; Yan, Y.; Gong, Y.; Zhang, X. Positive Charge of Chitosan Retards Blood Coagulation on Chitosan Films. *J. Biomater. Appl.* **2013**, *27*, 1032−1045.
(40) Lee, J. H.; Khang, G.; Lee, J. W.; Lee, H. B. Platelet Adhesion onto Chargeable Functional Group Gradient Surfaces. *J. Biomed. Mater. Res.* **1998**, *40*, 180−186.
(41) Lee, H. J.; Hong, J.-K.; Goo, H. C.; Lee, W. K.; Park, K. D.; Kim, S. H.; Yoo, Y. M.; Kim, Y. H. Improved Blood Compatibility and Decreased VSMC Proliferation of Surface-Modified Metal Grafted with Sulfonated PEG or Heparin. *J. Biomater. Sci., Polym. Ed.* **2002**, *13*, 939−952.
(42) Zandén, C.; Voinova, M.; Gold, J.; Mörsdorf, D.; Bernhardt, I.; Liu, J. Surface Characterisation of Oxygen Plasma Treated Electrospun Polyurethane Fibres and Their Interaction with Red Blood Cells. *Eur. Polym. J.* **2012**, *48*, 472−482.

(43) Eriksson, L. On the Shape of Human Red Blood Cells Interacting with Flat Artificial Surfaces—the 'Glass Effect'. *Biochim. Biophys. Acta* **1990**, *1036*, 193−201.
(44) Andrews, D. A.; Low, P. S. Role of Red Blood Cells in Thrombosis. *Curr. Opin. Hematol.* **1999**, *6*, 76.
(45) Cheng, C.; Li, S.; Nie, S.; Zhao, W.; Yang, H.; Sun, S.; Zhao, C. General and Biomimetic Approach to Biopolymer-Functionalized Graphene Oxide Nanosheet through Adhesive Dopamine. *Biomacromolecules* **2012**, *13*, 4236−4246.
(46) Kumar, S.; Dory, Y. L.; Lepage, M.; Zhao, Y. Surface-Grafted Stimuli-Responsive Block Copolymer Brushes for the Thermo-, Photo- and pH-Sensitive Release of Dye Molecules. *Macromolecules* **2011**, *44*, 7385−7393.
(47) Wang, C.-C.; Su, C.-H.; Chen, C.-C. Water Absorbing and Antibacterial Properties of *N*-Isopropyl Acrylamide Grafted and Collagen/Chitosan Immobilized Polypropylene Nonwoven Fabric and Its Application on Wound Healing Enhancement. *J. Biomed. Mater. Res., Part A* **2008**, *84A*, 1006−1017.
(48) Aranda, F. J.; Coutinho, A.; Berberan-Santos, M. N.; Prieto, M. J. E.; Gómez-Fernández, J. C. Fluorescence Study of the Location and Dynamics of α-Tocopherol in Phospholipid Vesicles. *Biochim. Biophys. Acta* **1989**, *985*, 26−32.
(49) Constantinides, P. P.; Han, J. H.; Davis, S. S. Advances in the Use of Tocols as Drug Delivery Vehicles. *Pharm. Res.* **2006**, *23*, 243−255.
(50) Guo, Y.; Luo, J.; Tan, S.; Otieno, B. O.; Zhang, Z. The Applications of Vitamin E TPGS in Drug Delivery. *Eur. J. Pharm. Sci.* **2013**, *49*, 175−186.
(51) Han, S. K.; Kim, M.; Park, Y. H.; Park, E. J.; Lee, J. H. Effect of Lipid Peroxidation on the Fluidity of Erythrocyte Ghost and Phospholipid Liposomal Membranes. *Arch. Pharmacal Res.* **1992**, *15*, 309−316.
(52) Nogueira, D. R.; Mitjans, M.; Busquets, M. A.; Pérez, L.; Vinardell, M. P. Phospholipid Bilayer-Perturbing Properties Underlying Lysis Induced by pH-Sensitive Cationic Lysine-Based Surfactants in Biomembranes. *Langmuir* **2012**, *28*, 11687−11698.
(53) Perutz, M.; Muirhead, H.; Cox, J.; Goaman, L.; Mathews, F.; McGandy, E.; Webb, L. Three-Dimensional Fourier Synthesis of Horse Oxyhaemoglobin at 2.8 Resolution:(I) X-Ray Analysis. *Nature* **1968**, *219*, 29−32.
(54) Drummen, G. P. C.; van Liebergen, L. C. M.; Op den Kamp, J. A. F.; Post, J. A. C11-Bodipy581/591, an Oxidation-Sensitive Fluorescent Lipid Peroxidation Probe: (Micro)Spectroscopic Characterization and Validation of Methodology. *Free Radical Biol. Med.* **2002**, *33*, 473−490.
(55) Aitken, R. J.; Wingate, J. K.; De Iuliis, G. N.; McLaughlin, E. A. Analysis of Lipid Peroxidation in Human Spermatozoa Using Bodipy C11. *Mol. Hum. Reprod.* **2007**, *13*, 203−211.
(56) Wattamwar, P. P.; Mo, Y.; Wan, R.; Palli, R.; Zhang, Q.; Dziubla, T. D. Antioxidant Activity of Degradable Polymer Poly(trolox ester) to Suppress Oxidative Stress Injury in the Cells. *Adv. Funct. Mater.* **2010**, *20*, 147−154.
(57) Xia, T.; Kovochich, M.; Brant, J.; Hotze, M.; Sempf, J.; Oberley, T.; Sioutas, C.; Yeh, J. I.; Wiesner, M. R.; Nel, A. E. Comparison of the Abilities of Ambient and Manufactured Nanoparticles To Induce Cellular Toxicity According to an Oxidative Stress Paradigm. *Nano Lett.* **2006**, *6*, 1794−1807.
(58) Mittler, R. Oxidative Stress, Antioxidants and Stress Tolerance. *Trends Plant Sci.* **2002**, *7*, 405−410.
(59) Xie, Q.; Li, S.; Feng, W.; Li, Y.; Wu, Y.; Hu, W.; Huang, Y. Inhibition of Monosodium Urate Monohydrate-Mediated Hemolysis by Vitamin E. *Acta Biochim. Biophys. Sin.* **2007**, *39*, 273−277.
(60) Labow, R. S.; Card, R. T.; Rock, G. The Effect of the Plasticizer Di(2-Ethylhexyl)Phthalate on Red Cell. *Blood* **1987**, *70*, 319−323.
(61) Sadrzadeh, S. M.; Graf, E.; Panter, S. S.; Hallaway, P. E.; Eaton, J. W. Hemoglobin. Hemoglobin. A Biologic Fenton Reagent. *J. Biol. Chem.* **1984**, *259*, 14354−14356.